

Research Paper

Rational design of temperature-sensitive blood-vessel-embolic nanogels for improving hypoxic tumor microenvironment after transcatheter arterial embolization

Ling Li^{1,3*}, Yiming Liu^{2,3*}, Han Li^{1,3*}, Xiaopeng Guo², Xiaojun He², Shinan Geng^{1,3}, Hao Zhao^{1,3}, Xiaole Peng^{1,3}, Dingwen Shi¹, Bin Xiong², Guofeng Zhou², Yanbing Zhao^{1,3}, Chuansheng Zheng², Xiangliang Yang¹

1. National Engineering Research Center for Nanomedicine, College of Life Science and Technology, Huazhong University of Science and Technology, 430074, Wuhan City, P. R. China.
2. Hubei Province Key Laboratory of Molecular Imaging, Department of Radiology, Union Hospital, Tongji Medical College, Huazhong University of Science and Technology, Wuhan 430022, China.
3. Shenzhen Institute of Huazhong University of Science and Technology, 518057, Shenzhen, P. R. China

*These authors contributed equally to this work.

 Corresponding author: Yanbing Zhao (zhaoyb@hust.edu.cn), Chuansheng Zheng (hqzcsxh@sina.com) and Xiangliang Yang (yangxl@hust.edu.cn); Tel: +86-27-87792147, Fax: +86-27-87792234.

© Ivyspring International Publisher. This is an open access article distributed under the terms of the Creative Commons Attribution (CC BY-NC) license (<https://creativecommons.org/licenses/by-nc/4.0/>). See <http://ivyspring.com/terms> for full terms and conditions.

Received: 2018.07.29; Accepted: 2018.11.14; Published: 2018.11.29

Abstract

Transcatheter arterial embolization (TAE) plays an important role in clinical tumor therapy by accomplishing vessel-casting embolization of tumor arteries at all levels and suppressing tumor collateral circulation and vascular re-canalization. In this study, we describe smart blood-vessel-embolic nanogels for improving the anti-tumor efficacy of TAE therapy on hepatocellular carcinoma (HCC).

Methods: In this study, an *in vitro* model composed of two microfluidic chips was used for simulating the tumor capillary network and analyzing artery-embolization properties. Also, blood-vessel-casting embolization of renal arteries was evaluated in normal rabbits. Using a VX2 tumor-bearing rabbit model, the therapeutic efficacy of TAE on HCC was investigated for tumor growth, necrosis, and proliferation. Neovascularization and collateral circulation were evaluated by immunofluorescent detection of hypoxia-inducible factor-1 α (HIF-1 α), vascular endothelial growth factor (VEGF), and CD31 following the TAE therapy of VX2 tumor-bearing rabbits.

Results: Sufficient embolization of all eight levels of micro-channels was achieved in a tumor-vessel-mimetic model with two microfluidic chips using PIBI-2240, and was further confirmed in renal arteries of normal rabbit. Effective inhibition of tumor collateral circulation and vascular re-canalization was observed in VX2 tumor-bearing rabbits due to the reduced expression levels of HIF-1 α , VEGF, and CD31.

Conclusions: The exceptional anti-tumor effect of PIBI-2240 observed in this study suggested that it is an excellent blood-vessel-embolic material for tumor TAE therapy.

Key words: Temperature-sensitive, Nanogel, Transcatheter arterial embolization, hypoxic microenvironment

Introduction

Transcatheter arterial embolization (TAE), which can selectively deliver embolic agents and drugs to target arteries under the guidance of medical imaging

equipment, plays an important role in the interventional therapy of a wide range of diseases including solid tumors, hemorrhages, and

arterio-venous malformations [1-3]. For example, TAE combined with intra-arterial delivery of chemotherapeutic agents (transcatheter arterial chemo-embolization, TACE) is recommended as a gold standard of first-line clinical palliative therapy for unresectable hepatocellular carcinoma (HCC) [4-7]. Embolic materials play a key role in TACE therapy of HCC, and can help achieve efficient loading and targeted delivery of chemo-therapeutics to occlude the arterial blood supply to the tumor. However, previous studies have shown that TACE could not achieve total necrosis of HCC leading to relapse and metastasis [1, 8]. Although TACE inhibited HCC by inducing local ischemia and hypoxia, only subtle effects of hypoxia were observed on the tumor microenvironment [9, 10]. For instance, embolization-inducing hypoxia is an important driving force in tumor progression by activated hypoxia-inducible factor-1 α (HIF-1 α) and vascular endothelial growth factor (VEGF) and is associated with tumor recurrence and metastasis [11, 12]. This complex effect is highly dependent on the extent and duration of hypoxia induced by embolization. Usually, severe and long-term hypoxia is beneficial to TACE therapy of HCC, whereas mild/short hypoxia increases the expression of HIF-1 α and VEGF [9, 13-14].

Clinical blood-vessel-embolic materials often cause insufficient embolization because of the heterogeneity of tumor vasculature and limitations of the TACE procedure [15-17]. To suppress the elevated expression of HIF-1 α and VEGF, blood-vessel-casting embolization of all tumor-feeding arteries must be accomplished in TACE therapy of HCC. The embolic materials must have two conflicting properties: flowability and embolization. For example, Lipiodol (Lipiodol Ultra-Fluid), by virtue of its good flowability, can diffuse rapidly into fine tumor arteries [18, 19]. Although Lipiodol is widely used in TACE clinical therapy and can cut-off tumor blood supply in a short time, it is difficult to achieve long-term embolization of tumor arteries due to blood scouring and rapid *in vivo* elimination. Gelfoam is the most commonly used particulate material to prolong the embolic time after Lipiodol injection, but results in complete re-canalization in one to two weeks [20-22]. Therefore, tumor recurrence and metastasis are often observed in patients receiving Lipiodol-based TACE therapy [23]. In contrast, granular/solid embolic materials, such as Ivalon, exhibit excellent resistance against the scouring of blood flow and can occlude tumor arteries over a long period of time. However, Ivalon is rarely used in TACE therapy of HCC because of its poor flowability, making it impossible to be delivered into peripheral arteries; these irregular

particles are designed for more proximal blockage and not deeper flow in the vessels [24]. The dilemma between flowability and embolization of blood-vessel-embolic materials caused tumor collateral circulation and/or vascular re-canalization, limiting the anti-tumor efficacy of TACE therapy [25-28].

To address the issue of flowability and embolization in the embolic materials, poly(N-isopropylacrylamide-co-butyl methylacrylate) (PIB) nanogels have previously been used for TACE therapy of HCC through temperature-sensitive sol-gel phase transition [28-34]. However, in this respect, tumor microenvironment did not receive enough attention so far. In the present work, complex dispersions of PIB nanogels and iohexol were further optimized to address the problem of increasing viscosity caused by mixing with iohexol [35-38]. The reduction of flowability may contribute to the hypoxic microenvironment (HIF-1 α , VEGF, etc) of tumors [39-42]. The temperature-sensitive sol-gel phase transition and rheological properties of the improved complex dispersions (PIBI-2240) were compared to those of Lipiodol, Ivalon, and original dispersions (PIBI-6150) [43]. In particular, an *in vitro* model composed of two microfluidic chips for simulating a tumor capillary network was used to study the artery-embolization properties of PIBI-2240 [44, 45]. Furthermore, *in vivo* renal arterial embolization was implemented in normal rabbits to evaluate blood-vessel-casting embolization of all levels of renal arteries [46, 47]. Using a VX2 tumor-bearing rabbit model, the therapeutic efficacy of TAE on HCC was investigated between Ivalon and Lipiodol in terms of tumor growth, necrosis, and proliferation. To investigate the influence of artery-embolization properties on the tumor microenvironment, we evaluated neovascularization and collateral circulation through immunofluorescent detection of HIF-1 α , VEGF, and CD31 after TAE therapy in VX2 tumor-bearing rabbits (Scheme 1).

Methods

Materials

PIB nanogels were prepared using emulsion polymerization as previously reported [28]. N-isopropylacrylamide (NIPAM; Tokyo Chemical Industry, Tokyo, Japan) and N,N'-methylenebisacrylamide (MBA; Sinopharm Chemical Reagent Co., Ltd.) were re-crystallized from n-hexane and methanol, respectively. Potassium persulfate (KPS; Sinopharm Chemical Reagent Co., Ltd.), sodium dodecyl sulphate (SDS; Sinopharm Chemical Reagent Co., Ltd.), dimethylformamide

(DMF; Sinopharm Chemical Reagent Co., Ltd.), 2-aminoethyl methacrylate hydrochloride (AM; J&K Scientific, Ltd.) and Cy5.5 NHS ester (Cy5.5; Lumiprobe Corporation, USA) were used directly without further purification. Butyl methacrylate (BMA; Sinopharm Chemical Reagent Co., Ltd.) was distilled before use. Iohexol (Omnipaque), Ivalon (PVA foam embolization particles, 180–300 μm), Gelfoam particles (180–300 μm) and Lipiodol (Lipiodol Ultra-Fluid) were purchased from Sigma-Aldrich (Darmstadt, Germany), Cook Medical (Bloomington, IN, USA) and Guerbet Pharmaceutical Production Plant (France), respectively. Milli-Q ultrapure water (18.2 M Ω) was used in all experiments.

Adult New Zealand white rabbits (weight: 2.5–3.0 kg, both sexes) were purchased from the Laboratory Animal Center of Huazhong University of Science and Technology. All procedures were in accordance with China National Animal Law on the use of laboratory animals.

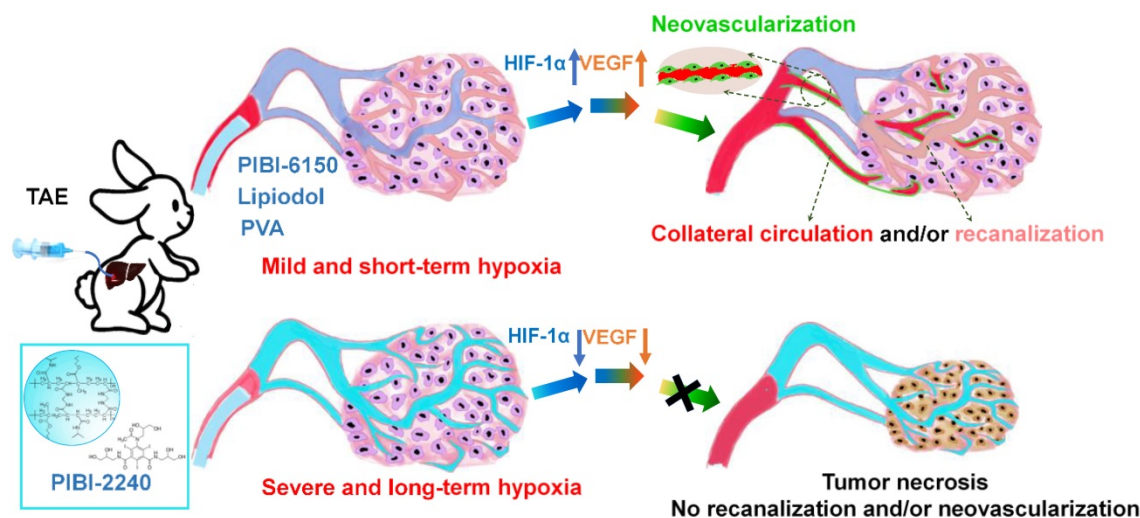
Preparation of the nanogels labeled with fluorescence dye Cy5.5

The near-infrared fluorescence dye Cy5.5 was conjugated with PIB nanogels. First, PIB nanogels composed of amino groups were synthesized by emulsion polymerization. Briefly, NIPAM (2.26 g, 20 mmol), BMA (168 μL , 1.0 mmol), AM (9 mg, 0.05 mmol), MBA (32 mg, 0.2 mmol) and SDS (32 mg, 0.12 mmol) were dissolved in 160 mL of ultrapure water. The mixing solution was heated to 70 $^{\circ}\text{C}$ under an N_2 atmosphere while stirring. 10 mL of a KPS solution (95 mg, 0.35 mmol) was rapidly added to the mixing solution to initiate polymerization. After reacting at 70 $^{\circ}\text{C}$ under an N_2 atmosphere for 4.5 h, the resultant nanogels were dialyzed (cut-off molecular

weight: 14 kDa) for one week, lyophilized and then stored in a desiccator at room temperature. The lyophilized nanogels (ca. 100 mg) were dispersed in a mixing solvent of $\text{H}_2\text{O}/\text{DMF}$ (volume ratio: 2:1, 30 mL) while stirring for 24 h. Subsequently, Cy5.5 NHS ester (ca. 3.0 mg) was added to the nanogel dispersions and conjugated with the amino groups in the nanogels under stirring for 8 h in the dark. The resultant nanogels labeled with Cy5.5 (Cy5.5-PIB nanogels) were dialyzed (cut-off molecular weight: 14 kDa) in the mixed solution of $\text{H}_2\text{O}/\text{DMF}$ (volume ratio: 2:1) and ultrapure water for three days to remove the unreacted Cy5.5 NHS ester and other small molecules. Finally, Cy5.5-PIB nanogels were lyophilized and stored in a desiccator at room temperature for further use.

Complex dispersions of PIB nanogels with iohexol (PIBI)

Complex dispersions of PIB nanogels with various concentrations of iohexol were prepared for the *in vitro/in vivo* comparison of TAE anti-tumor efficacy. Cy5.5-PIB nanogels and/or PIB nanogels (200 mg) were added slowly to 10 mL of an iohexol solution (240 mg I/mL). To ensure good nanogel dispersions in iohexol, the nanogel dispersions and iohexol were mixed at a low speed in an ice-water bath for at least 24 h. The complex dispersion of PIB nanogels (2.0 w/v%) with iohexol (iodine concentration, 240 mg/mL) was named PIBI-2240. Similarly, PIBI-2050, PIBI-2150 and PIBI-2350 had iodine concentrations of 50 mg I/mL, 150 mg I/mL and 350 mg I/mL, respectively, and a nanogel concentration of 2%. Also, PIBI-6150 had nanogel and iodine concentrations of 6.0 w/v% and 150 mg I/mL, respectively.



Scheme 1. Schematic design of the temperature-sensitive blood-vessel-embolic nanogels (PIBI-2240) for improving hypoxic tumor microenvironment after transcatheter arterial embolization.

Characterization

The size and zeta potentials (0.2 wt.% of nanogel concentration in ultrapure water) were measured using dynamic light scattering (Zetasizer Nano ZS90, Malvern Instruments Ltd., Malvern, UK) with a He-Ne laser source ($\lambda = 633$ nm, scattering angle: 90°). The nanogel morphologies were characterized using a transmission electron microscope (TEM; Tecnai G2 20, FEI Corp., Eindhoven, The Netherlands) at 200 kV. Two drops of nanogel dispersions (0.05 wt.%) were added on two carbon-coated copper grids and dried at 25°C and 37°C . A phosphotungstic acid solution (0.1 wt.%) was used as a staining agent. X-ray attenuation evaluation was performed using computed tomography (CT) scanner (SOMATOM Sensation 64 Spiral; Siemens) at 100 kV and 120 mA in body PCT mode. The X-ray mode of an IVIS Lumina XR system (Caliper Life Sciences, Hopkinton, MA, USA) was used for X-ray attenuation determination. 100 μL of PIBI dispersions and various concentrations of Omnipaque were added to a 96-well plate, and the entire region of each well was selected as the region of interest (ROI) for the sample in the well. The gray value of the ROI was measured using the built-in Living Image[®] software for X-ray attenuation evaluation.

Temperature-sensitive sol-gel transition and *in vitro* evaluation of artery-embolization properties

Temperature-sensitive sol-gel transition of various PIBI dispersions was investigated using phase diagram and rheological measurements. The phase diagrams of temperature versus nanogel and iodine concentrations were drawn using the inverted-vial method at a temperature range from 5°C to 45°C . The samples were maintained for 5 min at each temperature point. The rheological properties, including viscosity and visco-elasticity, were measured using a rheometer (Kinexus Ultra+, Malvern Instruments Ltd.) with a parallel plate (PP50, $\Phi = 50$ mm; the gap was set at 0.5 mm). The viscosities of the PIBI dispersions were measured at 25°C , and the shear rate was maintained at 300/s. Determination of temperature-sensitive visco-elasticity was performed in the temperature range from 23°C to 45°C with the following parameters: shear stress = 0.5 Pa, heating rate = $2^\circ\text{C}/\text{min}$, frequency = 1.0 Hz.

To investigate the artery-embolization behavior of various PIBI dispersions, a biomimetic model of a tumor arterio-capillary bed was designed with two PDMS microfluidic chips in parallel. According to the fractal structure of tumor vasculature networks,

eight-generation branching networks were etched in a silicon wafer using the technique of lithography, and a circuit system was formed with reversed eight-generation branching networks. Based on Murray's law [48], the sizes of eight micro-channels in the chips were $\Phi 800$, $\Phi 630$, $\Phi 500$, $\Phi 400$, $\Phi 300$, $\Phi 200$, $\Phi 100$, and $\Phi 20$ μm . PBS was driven by a fluid pump (high-performance liquid chromatography; Agilent 1260, Agilent Technologies) in the circuit system. The embolic agent was injected into the circuit system through a three-way valve. In the embolic process, the pressure was monitored in real time by a pressure gage. To avoid damaging the embolized chip by extremely high pressure, the same chip without embolization was used as a pressure control system. The *in vitro* artery-embolization device was kept at 37°C throughout the whole experimental period. PBS was circulated in the device for 1 h at a flow rate of 0.1 mL/min to remove the bubbles in the multi-channels of the chips. Subsequently, the embolic agents were injected at a rate of 0.5 mL/min, while continually washing with PBS for 60 min. Methylene blue was used to stain various PIBI dispersions for easy observation. The micrograph of the channels is taken using a Leica microscope (Leica, Bensheim, Germany).

In vivo antitumor evaluation of TAE therapy using PIBI dispersions on VX2 tumor-bearing rabbits

First, 48 normal New Zealand rabbits were randomly divided into four groups (12 rabbits per group), and renal arterial embolization was performed on the right kidney of normal rabbits with 2.5 mL of PIBI-6150, PIBI-2240, Ivalon, or Lipiodol. After abstaining from eating and drinking for 12 h, the rabbits were anesthetized by injecting 30 mg/kg pentobarbital sodium through their auricular veins and fixed in the supine position after pain sensation has diminished in 5–10 min. Their groin skin was dissected, and the femoral arteries were separated using ophthalmic forceps. Following ligation of the distal arteries, a 4F coaxial micro-catheter (Terumo, Tokyo, Japan) was introduced into the proximal arteries using an 18 G puncture needle. Renal arterial angiography was performed on rabbits after injecting a contrast agent (Omnipaque, 300 mg I/mL, 0.5 mL/s). PIBI-6150, PIBI-2240, Ivalon, or Lipiodol were injected into the right renal arteries, and the efficiency of renal arterial embolization was evaluated by histopathology and digital subtraction angiography (DSA; Siemens BICOR T.O.P., Germany) at 10 min, 1, 3, and 6 weeks after treatment. To evaluate *in vivo* embolization of various levels of the renal arteries, Cy5.5-labeled PIBI-2240 or

Cy5.5-labeled PIBI-6150 was used to occlude rabbit renal arteries for 1 h. The kidneys embolized with the Cy5.5-labeled nanogels were excised and sectioned into 10-mm-thick slices after the rabbits were killed by intravenous injection of pentobarbital sodium (30 mg kg⁻¹). The slices were examined using a confocal laser scanning microscopy (Olympus FV1000, Tokyo, Japan), for evaluating the nanogel distribution in various levels of renal arteries.

The VX2 tumor model in adult New Zealand white rabbits (weight: 2.5–3.0 kg) was prepared as previously reported [28, 29]. Briefly, the rabbits were anesthetized intravenously with sodium pentobarbital (2.0 wt.%, 30 mg/kg). The livers of the rabbits were then exposed, and the resulting VX2 tumor particles that are 1.0 mm³ in size were transplanted into the left liver lobe. After 17 days of tumor implantation, 60 VX2 tumor-bearing rabbits were randomly divided into four groups (15 rabbits per group) and the TAE therapy of PIB dispersions in liver tumors was evaluated. The embolic material was injected at a rate of 0.5 mL/s. During the Ivalon-TAE procedure of the liver, 100 mg of Ivalon powder was pre-mixed with 10 mL of iohexol solution (350 mg I/mL), and approximately 0.25 mL of the mixture per rabbit was used in all Ivalon-TAE procedures. Also, Lipiodol/Gelfoam, PIBI-2240, and normal saline (ca. 0.3 mL per rabbit) were injected without any dilution because of their good flowability based on angiography.

At 0, 7, and 14 days after treatment, magnetic resonance imaging (MRI; Siemens MAGNETOM Avanto 1.5T, Erlangen, Germany) was used to analyze the tumor growth rate (GR) with a body matrix coil, and T2-weighted images were acquired using the turbo spin-echo sequence (TR/TE, 3,700/87 ms, BW, 168 Hz/pixel; matrix: 320 × 320). The section thickness and intersection gaps were 4 mm and 15%, respectively, and the view field was 200 × 200 mm. The GR of the liver tumor was calculated as follows: $GR = a_2 b_2^2 / a_1 b_1^2$, where a_1 and a_2 are the maximum diameters, and b_1 and b_2 are the minimum diameters of the tumor before and after TAE treatment, respectively. The tumor necrosis rate (TNR) was calculated by the area percentage of the necrotic region in the total region of the tumor, which was calculated as follows from hematoxylin and eosin (H&E) stained sections:

$$TNR = \left[\frac{n}{n+t} \right] \times 100,$$

where n is the necrotic area and t is the tumor cell area [49, 50]. In addition, the relative body weight (RBW %) was calculated using the following equation:

$$RBW\% = \frac{w_t - w_0}{w_0} \times 100,$$

where w_0 and w_t are the body weight of rabbits before and after t days of treatment, respectively.

Evaluation of histopathology and immunofluorescence

Histopathological analyses, such as H&E staining, terminal deoxynucleotidyl transferase dUTP nick-end labeling (TUNEL), and immunohistochemical staining, were further used to investigate the anti-tumor effect of TAE treatment. After TAE therapy of VX2 tumor-bearing rabbits or normal rabbits, the rabbits were humanely killed to collect various samples, including tumor, peri-tumoral liver, and kidney tissues at various time intervals. All tissue samples were fixed in 10% buffered formalin, embedded in paraffin and cut into slices. The slides were de-waxed in xylene, hydrated using graded ethanol and stained for routine histologic evaluation by H&E. The sections were then observed microscopically (Leica DM3000). The TUNEL assay was used to stain and quantify apoptotic cells in tissue sample slices according to the manufacturer's protocol. Briefly, the slices were incubated with proteinase K (20 µg/mL) at 37 °C for 20 min, rinsed with pure water, and then stained with TUNEL (1 : 9; Roche Diagnostics GmbH, Mannheim, Germany) at 37 °C for 1 h in the dark. Subsequently, the slices were stained for 5 min with 4',6-diamidino-2-phenylindole dihydrochloride (DAPI). CLSM (Eclipse Ti; Nikon Corporation, Tokyo, Japan) was used to examine tumor cell apoptosis in various slices.

Before immunohistochemical analyses, the slices were immersed in a citrate buffer (0.01 mmol/L, pH = 6.0) and heated three times in a microwave oven (5 min each time). Endogenous peroxidase was blocked with methanol containing 3% hydrogen peroxide for 10 min. For various immunofluorescent analyses, the slices were incubated overnight at 4 °C with a 150-fold dilution of mouse anti-Ki67 antigen (Dako, Carpinteria, CA, USA), a 100-fold dilution of mouse anti-HIF-1α (Thermo, IL, USA), a 150-fold dilution of mouse anti-VEGF (Millipore, Billerica, MA, USA), and a 50-fold dilution of mouse anti-human CD31 (Dako, Copenhagen, Denmark) monoclonal antibodies. The slices were washed with PBS 3 times for 5 min each and incubated at 37 °C sequentially with a 150-fold dilution of goat anti-rabbit secondary antibody (Aspen, Wuhan, China) for 50 min and a 200-fold dilution of fluorescent secondary antibody fluorescein isothiocyanate (FITC) (1 : 200, Wuhan Servicebio Biological Technology Co., Ltd., Wuhan, China) or Cyanine 3 (Cy3) (1 : 50, Wuhan Servicebio Biological Technology Co., Ltd.) for 60 min. Lastly, the slices

were stained with DAPI to label the nuclei of tumor cells. CLSM (FV1000; Olympus) was used to investigate the expression levels of HIF-1 α , VEGF, and CD31 (Cy3, Ex/Em = 554 nm/650 nm; FITC, Ex/Em = 488 nm/525 nm; DAPI, Ex/Em = 350 nm/460 nm).

The image analysis software package, Image-Pro Plus 6.0 software (Media Cybernetics, Warrendale, PA, USA) was used to quantify the average fluorescent intensity of six regions of tissue images (magnification: 200 \times). Apoptosis, proliferation, and HIF-1 α were assessed as follows: Single cells were scored as positive when a fluorescence signal for a specific marker was detected, and values were expressed as % mean of positive cells with respect to the mean total number of nuclei. The percentage of VEGF and CD31 was calculated using the following formula [51]:

$$\text{Percentage of area with positive staining} = \frac{\% \text{ mean of VEGF or CD31 area}}{\text{Mean total ROI in samples}}$$

Biocompatibility evaluation

Cell cytotoxicity on the hepatoblastoma (HepG2) cell line was investigated by the MTT assay. Briefly, HepG2 cells were seeded in 96-well plates at 8 \times 10⁴ cells/well in DMEM. After incubation overnight, the media were replaced by the samples with various concentrations (diluted using DMEM) and incubated at 37 $^{\circ}$ C for 24 h. The negative control was the cells in DMEM, and the blank control was DMEM without cells. 20 μ L of MTT and 100 μ L of DMEM were added to each well, and the cells were incubated further for 4 h. The optical density (OD) value was determined using a microplate reader (1420 Multilabel Counter; PerkinElmer, Waltham, MA, USA) at 450 nm. Cell viability (CV) was calculated using the following equation:

$$\text{CV}\% = \frac{\text{OD}_s - \text{OD}_b}{\text{OD}_n - \text{OD}_b} \times 100,$$

where OD_s, OD_b, and OD_n are the OD values of samples, blank, and negative control, respectively.

Hemolysis evaluation was performed on New Zealand rabbits as previously described [52]. Briefly, the red cell suspension (RCS) was obtained by centrifuging (1,500 rpm \times 10 min \times 3 times) mixing rabbit whole blood and normal saline. 500 μ L of RCS was incubated at 37 $^{\circ}$ C for 1 h, and the supernatant was collected by centrifugation (10,000 rpm \times 25 min) to determine the OD using a microplate reader (λ = 540 nm; 1420 Multilabel Counter, PerkinElmer). Taking normal saline and ultrapure water as the negative and positive control, respectively, the hemolysis ratio (Hr%) was calculated using the following equation:

$$\text{Hr}\% = \frac{\text{OD}_s - \text{OD}_n}{\text{OD}_p - \text{OD}_n} \times 100,$$

where OD_s, OD_n, and OD_p are the OD values of samples, negative control and positive control, respectively.

A biochemical auto-analyzer was used to measure the liver and renal function (Model DXC 8000; Beckman Coulter Diagnostics, Brea, CA, USA). 2.0 mL of peripheral blood was collected on 1 (before), 3, 6, and 14 days after the TAE therapy. Plasma alanine aminotransferase (ALT), aspartate aminotransferase (AST), blood urea nitrogen (BUN) and serum creatinine (CRE) were also measured.

Statistical Methods

All data were presented as the mean \pm standard deviation for at least three independent experiments. The measurement data were analyzed statistically using the independent-samples t-test and double-factor variance analysis, and the enumeration data were analyzed by chi-square (χ^2) and Fisher's exact probability tests. The results were considered statistically significant at a P-value of <0.05.

Results and discussion

Preparation and characterization of PIBI-2240

To address the issue of flowability and embolization, we had previously developed temperature-sensitive PIB nanogels as smart materials for embolization [28]. As shown in the TEM images (Figure 1A), PIB nanogels were regularly spherical with a hydrodynamic diameter of ca. 210 nm at 25 $^{\circ}$ C and 88.5 nm at 37 $^{\circ}$ C. The nanogel volume was reduced ca. 13.5 times due to the hydrophilic-hydrophobic transition with temperature, which was greatly influenced by the polarity of the media. The low critical solution temperature (LCST) of nanogels, which was used to characterize the temperature-sensitive hydrophilic-hydrophobic transition behavior, increased from 25 $^{\circ}$ C to 31 $^{\circ}$ C as the amount of the added hydrophilic iohexol (an X-ray contrast in clinical use) increased from 50 mg I/mL to 350 mg I/mL (Figure 1B). This was consistent with the reported results where the LCST of temperature-sensitive polymers increased with hydrophilic compounds but decreased with hydrophobic compounds [53].

To investigate the flowability of PIBI dispersions, their viscosities were compared under a wide range of shear rates (0.01–2,000/s) with Lipiodol, one of the most commonly used liquid embolic agents in TACE therapy of HCC. First, the typical characteristic of a Newtonian fluid, i.e., almost unchanged viscosity (ca.

100 mPa s) that does not depend on the shear rate in the range of 0.01–2,000/s, was determined using Lipiodol (Figure 1C). In contrast, a linear reduction of viscosity with the shear rate was exhibited using PIBI-6150 and PIBI-2240; the viscosity of PIBI-6150 decreased from 1.85×10^5 mPa s (0.01/s) to 135 mPa s (2,000/s), and that of PIBI-2240 decreased from 152 mPa s (0.01/s) to 18 mPa s (2,000/s). These are considered shearing-thinning properties, which are classical characteristics of non-Newtonian fluids. Furthermore, as calculated from the injection velocity (5–10 mL/min) of blood-embolic agents in clinical practice, the viscosity of PIBI-2240 was ca. 25 mPa s at the shear rate of 300/s, which was only a quarter and a thirteenth of those (94 and 328 mPa s) of Lipiodol and PIBI-6150, respectively (Table 1). This indicated that PIBI-2240 exhibited the best flowability in the arterial injection of these agents. In Figure 1D, the X-ray attenuation abilities of PIBI dispersions were compared with various iodine contents using the IVIS Lumina XR system in X-ray mode. Similar to that of the X-ray contrast iohexol, the grey values of PIBI dispersions increased from 1.74 at 50 mg I/mL to 3.78 at 350 mg I/mL. This showed that PIBI-2240 (3.44) and Lipiodol (3.77) exhibited the same ability of X-ray attenuation.

Table 1. Comparison of rheological properties of PIBI-2240, PIBI-6150, and Lipiodol at various temperatures

	Viscosity (mPa s) *	G25 (Pa, 25 °C) **	G (Pa, 37 °C)**	G37 / G25
Lipiodol	95	0.64	0.33	0.5
PIBI-6150	320	49.91	159.80	3.2
PIBI-2240	22	0.28	58.04	207.3

*: The viscosities of embolic agents were measured at 25 °C, and the shear rate was 300 s⁻¹.

** : G25 and G37 were the complex moduli of various embolic agents at 25 °C and 37

°C, respectively. They were defined as: $G = \sqrt{[(G')^2 + (G'')^2]}$ G' and G'' were the corresponding storage modulus and loss modulus of embolic agents at various temperatures.

Temperature-sensitive sol-gel phase transition and *in vitro*-simulated embolization behavior

Temperature-sensitive sol-gel phase transition, which is significantly influenced by mixing with iohexol, plays a crucial role in the TAE therapy of PIBI dispersions and is profoundly affected by additive compounds. For instance, the critical gelation concentration (CGC), which is defined as the critical temperature point of the sol-gel phase transition, usually occurs above 60 mg/mL for PIB nanogels [54]. However, as shown in Figure 1E, it decreased to ca. 10 mg/mL for PIBI dispersions when hydrophilic iohexol was added to an iodine concentration of 240 mg I/mL. This decrease was probably attributed to the fact that macroscopic three-dimensional

networks were formed by hydrogen bonding cross-linkages between iohexol molecules and nanogels. Moreover, there were only flowable sol (Phase 1) and shrunken gel (Phase 2) for PIBI dispersions in the concentration range of 10–50 mg/mL. As the nanogel concentration increased up to 50 mg/mL, an emerging swollen gel (Phase 0) could be detected below 10–20 °C. The influence of iohexol on the temperature-sensitive sol-gel transition behavior at 20 mg/mL nanogel concentration is displayed in Figure 1F. With the increasing concentration of iohexol, the critical gelation temperature (CGT) of flowable sol/shrunken gel transition slightly increased from 34.5 °C (50 mg I/mL) to 35.5 °C (200 mg I/mL) and then decreased to 32.5 °C (350 mg I/mL). Interestingly, the shrunken gel phase of PIBI dispersions gradually turned clear with the increase in iohexol content (Figure S1). Hence, iohexol could enhance the nanogel's hydrophilicity through hydrogen bonding. Furthermore, the rheological results (Figure 1G) indicated that the storage modulus G' (0.03–0.12 mPa s) and loss modulus G'' (0.06–0.44 mPa s) values of PIBI-2240 were very low in the flowable sol phase state (20–32 °C). In contrast, the G' (0.34–71.1 mPa s) and G'' (0.15–23 mPa s) values of PIBI-6150 were much higher than those of PIBI-2240 in the same temperature range (Figure 1H). Although PIBI-2240 had lower G' and G'' values in the flowable sol phase than those of PIBI-6150 as well as Lipiodol, its G' and G'' values in the shrunken gel phase reached up to 111.2 mPa s and 85 mPa s, respectively, very close to those of PIBI-6150 (152.1 and 122.2 mPa s). As shown in Figure 1I, the G' and G'' values of Lipiodol were only 0.33 mPa s and 0.02 mPa s, respectively, at 37 °C. The G37/G25 ratio, which was defined as the complex moduli ratio at 37 °C and 25 °C, was used to evaluate the properties of flowability and embolization at various temperatures. For instance, the G37/G25 ratio of PIBI-2240 was 207.3, much higher than those of PIBI-6150 (3.2) and Lipiodol (0.5) (Table 1). Therefore, PIBI-2240 had a much higher temperature sensitivity than those of PIBI-6150 and Lipiodol and thus exhibited the best properties of flowability and embolization among the three materials.

To investigate the *in vitro* artery-embolization properties of PIBI dispersions, a biomimetic model with two micro-fluidic chips was designed to simulate the tumor vasculature (Figure 2A). Hierarchical micro-channels with various widths (800, 630, 500, 400, 300, 200, 100, and 20 μm) were etched in two chips by lithography. Using PBS as a cycling medium, the artery-embolic materials were injected into one chip, which was used to simulate vascular networks, and the other chip was applied as a

pressure-controlled setup to prevent the damage to the vascular-simulated chip by extremely high pressure. Following injection at a rate of 0.5 mL/min, PIBI-2240 exhibited complete embolization of all eight levels of micro-channels from 20 to 800 μm (Figures 2A and S2). In contrast, PIBI-6150 showed partial embolization of the three finest channels (with widths of 20, 100, and 200 μm), indicating that it was difficult for PIBI-6150 to diffuse into very tiny capillaries (<200 μm) due to its higher viscosity. On the other hand, Lipiodol could also achieve complete embolization of all eight levels of micro-channels

because of its good flowability. However, as shown in Figures 2B and 2C, the kinetic change of pressure indicated that the complete embolization induced by Lipiodol only lasted a short time under the sustained elution with PBS. At an elution rate of either 0.1 mL/min or 0.3 mL/min, the embolization pressure of Lipiodol reached a maximum value at 0.5 min and then rapidly decreased to the pre-embolization pressure at about 2 min, while the embolization pressures of PIBI-2240 and PIBI-6150 maintained the maximum values during the entire PBS-eluting process (>60 min).

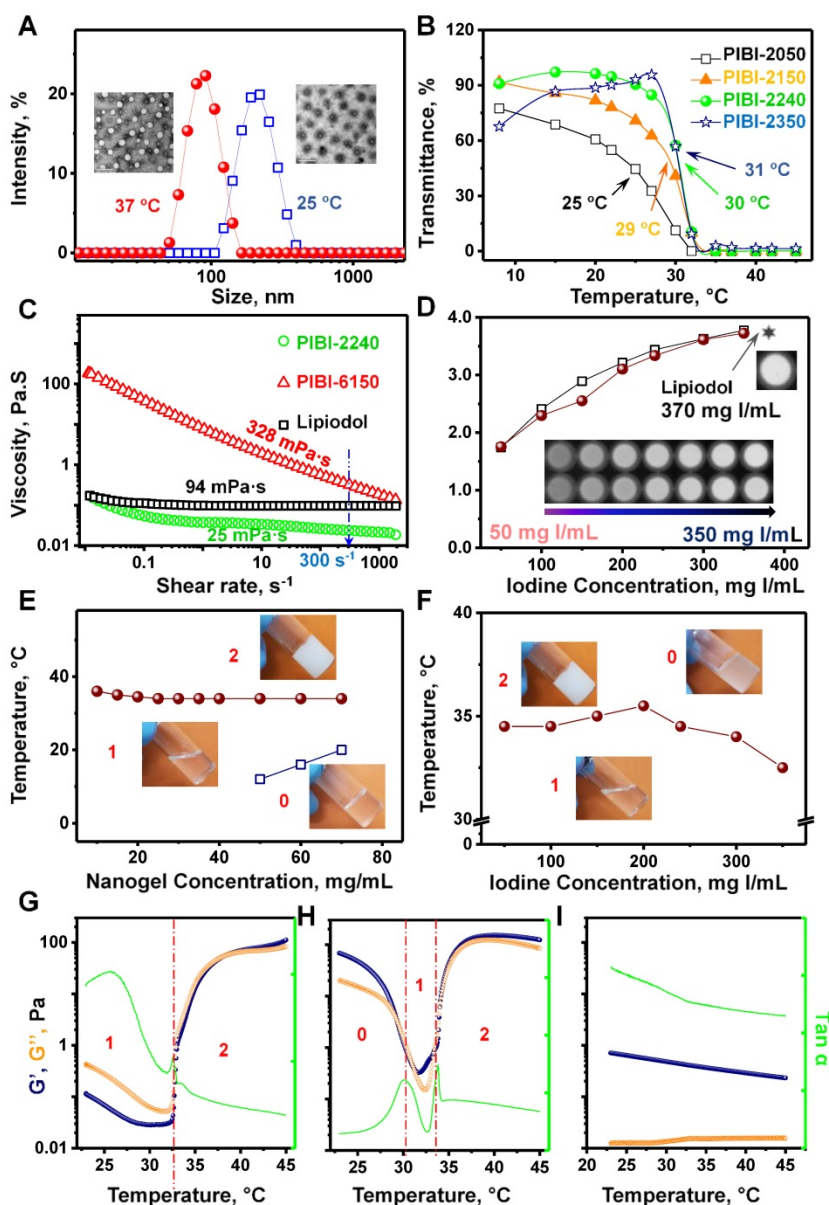


Figure 1. Properties of PIBI dispersions and temperature-sensitive sol-gel phase transition: (A) Hydrodynamic diameters of PIB nanogels measured by DLS at 25 °C (blue square and line) and 37 °C (red sphere and line). The inset pictures represent their TEM images, and the scale bar is 200 nm. (B) Temperature-sensitive transmittance of PIBI dispersions at various iodine concentrations (50, 150, 240, and 350 mg I/mL). The concentration of PIB nanogel was 2% (w/v). (C) Shear dependence on the viscosities of three Non-Newtonian fluids: PIBI-2240 (green solid sphere), PIBI-6150 (red hollow triangle) dispersions, and Lipiodol (black hollow square). (D) X-ray attenuation comparison of PIBI-2240 (burgundy solid sphere) with Lipiodol (black hollow square) at the same iodine content. (E) Phase diagram of the PIB nanogels vs temperature; iodine content was 240 mg I/mL. (F) Phase diagram of iodine content vs temperature. The concentration of PIB nanogels was 2.0 w/v%. (G), (H), and (I) are temperature-dependent rheological properties of PIBI-2240, PIBI-6150, and Lipiodol, respectively. Storage modulus G' (blue), loss modulus G'' (orange) and loss tangent $\text{Tan } \alpha$ (green).

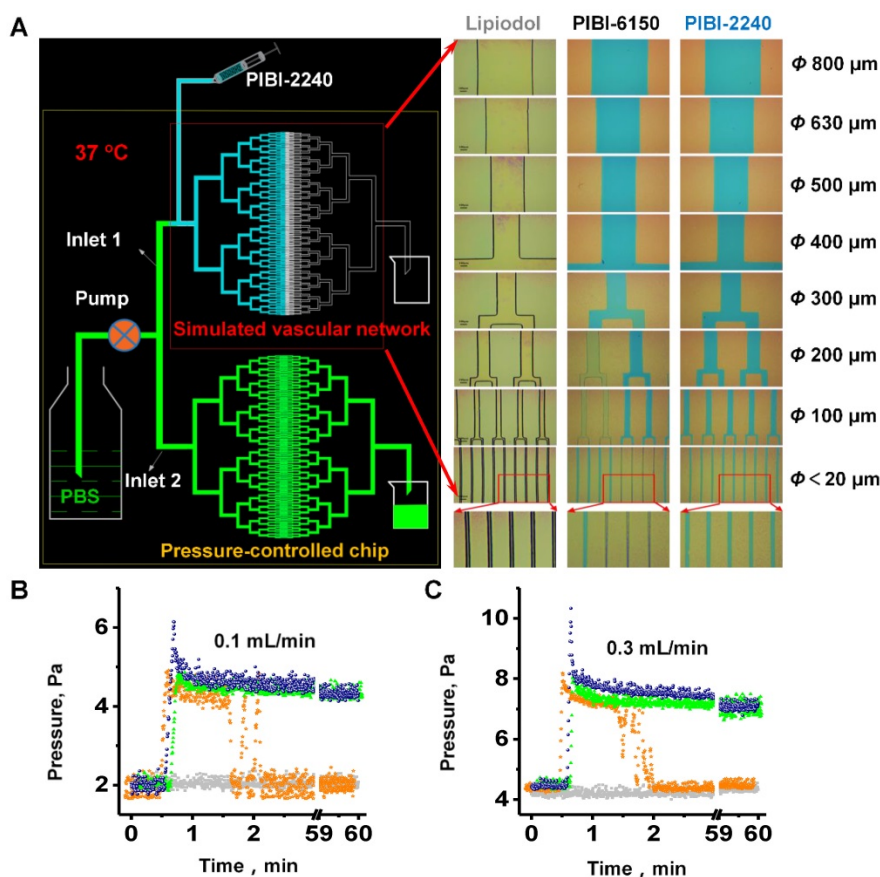


Figure 2. Artery-embolization comparison of PIBI-2240 with PIBI-6150 and Lipiodol by the *in vitro* model of vascular architecture networks. (A) The diagram of *in vitro* model of vascular architecture networks which was constituted by two microfluidic chips, and diffusion behavior of embolic agents in chip channels with various diameters. (B) and (C) are the pressure change curves of PIBI-2240 (dark blue), PIBI-6150 (green), Lipiodol (orange), and saline (gray) after *in vitro* embolization at the flow rates of 0.1 mL/min and 0.3 mL/min, respectively.

Renal arterial embolization in normal rabbits

We first performed *in vivo* artery embolization on the right kidney of a normal rabbit, since the abundant and hierarchical arteries in the kidney are beneficial for the precise evaluation of embolization to various arteries. Lipiodol-embolized arteries, including the renal aorta, inter-lobar arteries, and arcuate arteries, began to re-canalize at 10 min after treatment and were entirely opened on day 7 as confirmed by the black shadows in the DSA images (Figure 3A). Unlike Lipiodol, Ivalon (polyvinyl alcohol micro-particles) could occlude renal arteries for a long time. However, the black shadow still re-appeared in the arteries near the renal hilum 21 days after treatment, indicating that the arteries of the lower pole of the right kidney were opened again. The renal parenchyma could be imaged with DSA on day 21. In contrast, the black shadow immediately disappeared after the injection of PIBI-6150 and PIBI-2240 leading to a permanent renal arterial embolization as no re-canalization occurred in the embolized arteries for up to 42 days. This permanent renal arterial embolization induced numerous

necrotic spots on the embolized kidney and resulted in distinct renal atrophy compared to un-embolized kidneys. Although renal atrophy was also found in Ivalon-embolized kidneys, the renal aorta near the renal hilum was re-canalized in 21 days and resulted in incomplete renal atrophy (Figure S3).

The embolization abilities of PIBI-2240 and PIBI-6150 were further investigated in various levels of renal arteries. As shown in the fluorescent tissue section of the embolized kidney (Figure 3B), Cy5.5-labeled PIBI-2240 could diffuse easily into various levels of renal arteries, including the main renal arteries (MRAs), intra-renal arteries (IRAs) and even afferent renal arteries (ARAs) in the distal cortex of the kidney. Furthermore, Cy5.5-labeled PIBI-6150 was retained in MRAs and IRAs and was barely found in the finest peripheral arteries, such as ARAs. These results indicated that the excellent flowability of PIBI-2240 helped achieve complete embolization (also known as artery-casting embolization) of all levels of arteries from MRAs to IRAs and ARAs which is important for the inhabitation of tumor collateral circulation and the enhancement of the anti-tumor effect of TAE therapy.

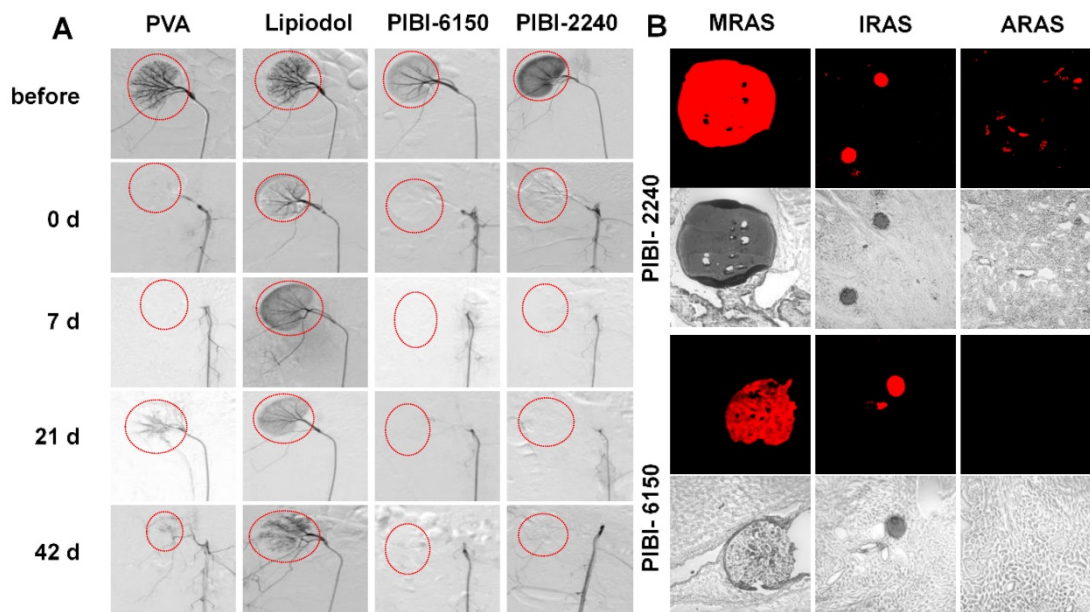


Figure 3. Renal artery embolization comparison of PIBI-2240 with PVA, Lipiodol, and PIBI-6150 in normal rabbits: (A) DSA images of rabbit kidney before and post-embolization on 0, 7, 21, and 42 days. Iohexol (350 mg I/mL) was used as a contrast for DSA. (B) Renal arterial embolization comparison of Cy5.5-labeled PIBI-2240 with Cy5.5-labeled PIBI-6150 using confocal fluorescence microscopy (original magnification, ×100). Main renal arteries (MRAs), intrarenal arteries (IRAs) and afferent renal arteries (ARAs).

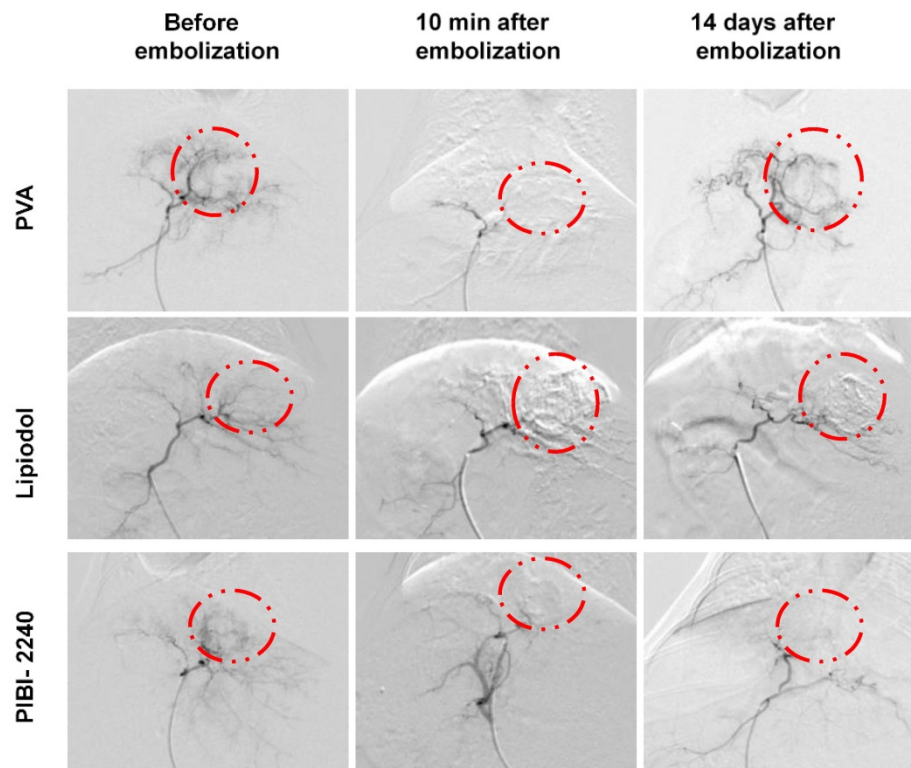


Figure 4. DSA images of the VX2 tumor at various times after treatment with PVA, Lipiodol, and PIBI-2240. The region surrounded by dotted red line is the tumor.

TAE therapy of PIBI-2240 on VX2 tumor-bearing rabbits

The TAE efficacy of PIBI-2240 was compared with that of Ivalon and Lipiodol in a VX2 tumor-bearing rabbit. As shown in the DSA images,

the black shadow, which was used to identify the tumor, disappeared immediately after treatment with PIBI-2240, Ivalon, or Lipiodol (Figure 4) indicating that these embolic agents could rapidly occlude the tumor blood supply. However, the black shadow re-appeared after 14 days in the DSA images of the

liver tumor embolized by Ivalon which indicated only partial embolization of large arteries and failure of embolization of the peripheral arteries leading to tumor collateral circulation. The black shadow was also found in the DSA images of the liver tumor 14 days after treatment with Lipiodol. However, no black shadows were found in the DSA images on day 14 when PIBI-2240 was used, demonstrating permanent embolization of all levels of arteries (from large arteries to peripheral arteries). The *in vivo* antitumor effect of TAE therapy was investigated in VX2-tumor-bearing rabbits for up to 14 days. As shown in Figures 5A and 5C, the tumor GR of rabbits treated with PIBI-2240 decreased to $100.7 \pm 6.0\%$ on day 7 and even to $92.6 \pm 34.7\%$ on day 14 after TAE therapy, far less than those treated with Lipiodol ($138.9 \pm 10.3\%$), Ivalon ($181.9 \pm 18.7\%$), and normal saline ($636.3 \pm 103.6\%$) for 14 days. Figures 5D and 5E indicated that the TNR, when treated with PIBI-2240, reached up to $81.0 \pm 4.8\%$ on day 14, also far higher than when treated with Lipiodol ($52 \pm 3.3\%$), Ivalon ($29.9 \pm 6.3\%$) and normal saline ($43.3 \pm 11.2\%$). In Figures 5B and 5F, an extensive necrotic area, tumor structural disorganization, and fewer surviving tumor cells were detected in the H&E-stained section of the VX2 tumor treated with PIBI-2240, whereas many surviving tumor nidi were found in tumors treated with Ivalon and Lipiodol. Moreover, TUNEL staining was performed on tumor tissue sections, where an increase in the green fluorescence indicated an increase in tumor cell death in the treatment groups. An increased level of green fluorescence of TUNEL-positive nuclei was observed only in PIBI-2240-treated tissue sections providing evidence of apoptotic cell death. Also, a definite decrease in tumor cell proliferation was evident from the decreased Ki67 expression in the PIBI-2240 treatment group compared with groups treated with Ivalon and Lipiodol (Figures 5E, 5F and 5G). The significant differences in tumor apoptosis and proliferation indicated that PIBI-2240 achieved full embolization of all levels of tumor arteries compared to Lipiodol and Ivalon and thus exhibited a stronger anti-tumor effect of TAE therapy as determined by the effective inhibition of tumor collateral circulation and vascular re-canalization.

The local hypoxia induced by insufficient TAE therapy is known to cause activation of HIF-1 α and thus increase the expression of VEGF. Positive HIF-1 α staining was noted in both the cytoplasm and nuclei of viable tumor cells. HIF-1 α -positive tumor cells were located predominantly at the periphery of necrotic tumor regions. As shown in Figures 6A and 6D, expression of HIF-1 α on day 14 in the saline group

was much lower than that in the groups treated with Ivalon and Lipiodol but much higher than that in the PIBI-2240 group, demonstrating significant differences in HIF-1 α expression among the three groups. Cytoplasmic VEGF expression was detected mainly in the viable tumor cells distributed at the periphery of necrotic tumor regions. The number of VEGF-positive cells was significantly increased in the saline, Ivalon, and Lipiodol groups compared with the PIBI-2240 group (Figures 6B and 6E). Microvessels were heterogeneously distributed in the tumors, and the most intense vascularization was observed in the invading edge of tumor margins. As displayed in Figures 6C, 6F, and 5H, expression of CD31 significantly increased on day 14 in the Ivalon and Lipiodol groups. The saline group exhibited a slight increase in the CD31 expression compared with the PIBI-2240 group in which the mean CD31 expression was significantly decreased. In VX2 tumors, HIF-1 α , as well as CD31 expression, showed a significantly positive correlation with VEGF-positive cells.

The purpose of embolization is to interrupt the blood flow to the tumors thereby inducing ischaemic necrosis and tumor hypoxia. Although hypoxia is toxic to cancer cells, the precise effect varies with its extent and duration. Severe and prolonged hypoxia induces cell death, whereas mild or short hypoxia can cause a series of adaptive genetic changes in cells. Results on the expressions of HIF-1 α , VEGF, and CD31 indicated that PIBI-2240 effectively limited neovascularization and collateral circulation compared to Ivalon and Lipiodol. This could be explained by the fact that PIBI-2240, due to its temperature-sensitive sol-gel transition, generated vessel-casting embolization of all levels of tumor vessels from the main to peripheral arteries.

PIBI-2240 also exhibited a satisfactory X-ray attenuation ability, whereas Ivalon and embolization microspheres utilized simple mixtures containing iodinated contrast media. However, PIBI-2240 demonstrated poor long-term imaging properties since the X-ray contrast (iohexol), which was used in PIBI-2240, was rapidly eliminated *in vivo*. Therefore, it was difficult to achieve a long-term CT examination post-operatively. The drug-loading and sustained-release behavior of PIBI-2240 were not investigated in the present study. However, as stated in the previous study, further investigations of the improvement of the TACE therapy of HCC are needed [29, 34]. A sustained-release period of 2–4 weeks of nanogels has been achieved which still needs to be improved to reach 3–6 months. Much effort is being devoted to improving the drug-loading amount and sustained-release behavior of PIBI-2240.

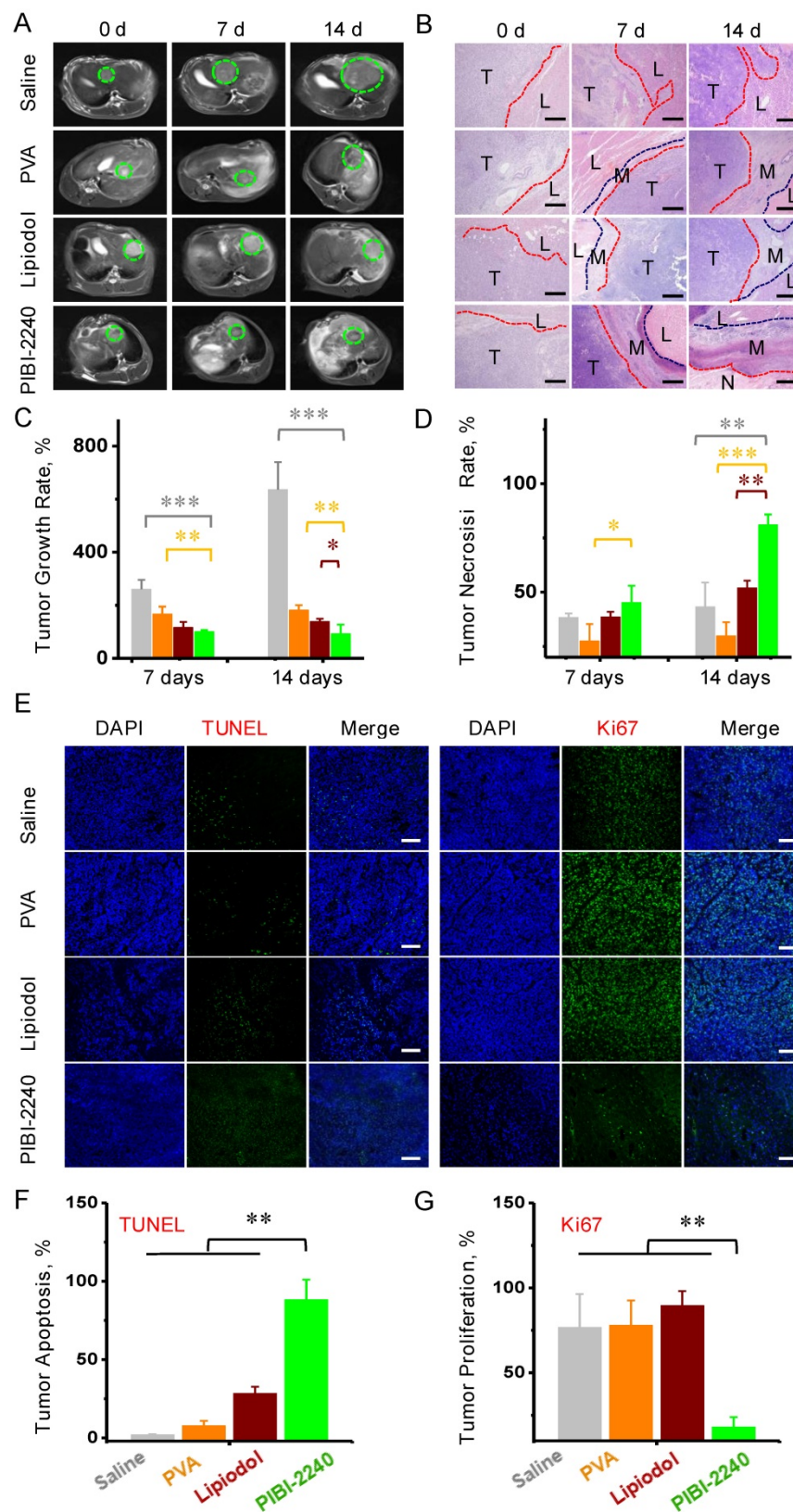


Figure 5. Antitumor efficacies of TAE therapy in VX2 tumor-bearing rabbits (A) MR images after 0, 7, and 14 days of embolization (green circle indicates the tumor region). (B) Histopathology with H&E staining after 0, 7, and 14 days of embolization, (T) areas of tumor (L) liver tissue (N) areas of necrosis (M) tumor margins. Scale bar: 500 μ m. (C) Tumor growth rate and (D) Tumor necrosis rate after TAE therapies with saline (gray), PVA (orange), Lipiodol (burgundy), and PIBI-2240 (green). (E) Confocal fluorescence microscopy images of cell apoptosis (stained by TUNEL) and cell proliferation (stained by Ki67) in histology sections of VX2-tumors following TAE therapies for 14 days. Scale bar: 100 μ m. (G) and (H) Quantitative analysis of fluorescence intensities of the images in Plot D with TUNEL and Ki67 staining, respectively. * $p < 0.05$, ** $p < 0.01$, and *** $p < 0.001$.

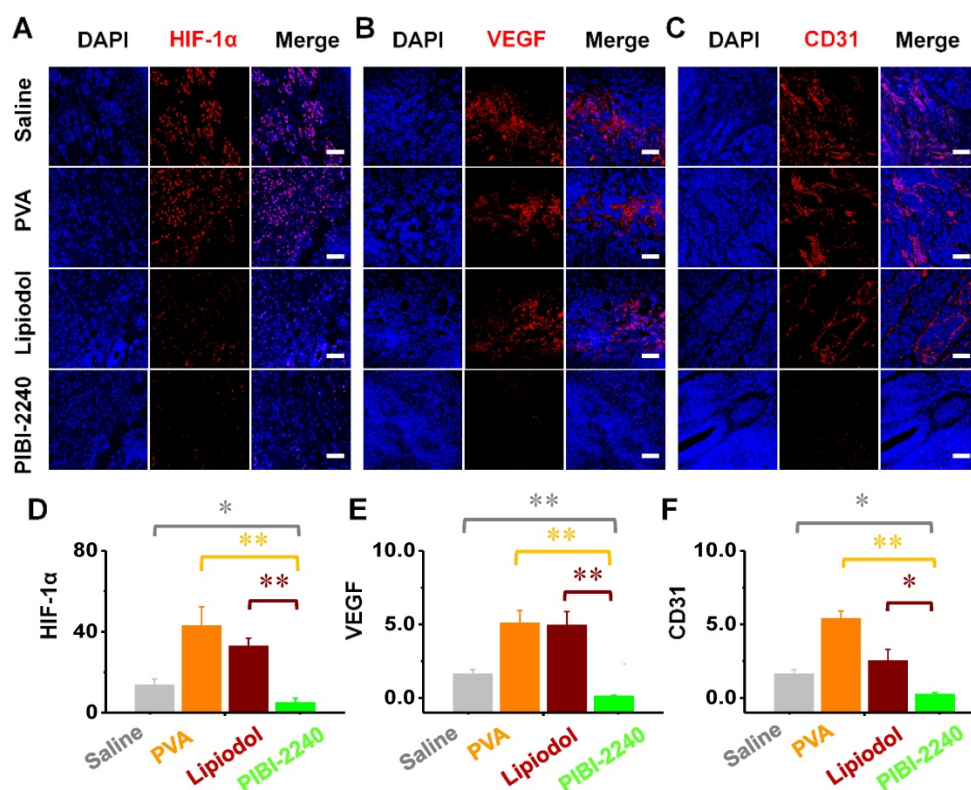


Figure 6. Immunofluorescence evaluations of neovascularization and collateral circulation in VX2 tumor-bearing rabbits after 14 days of blood-vessel-embolization with various materials (Saline, PVA, Lipiodol, and PIBI-2240). (A) Confocal fluorescence microscopy images of HIF-1 α staining. (B) Confocal fluorescence microscopy images of VEGF staining. (C) Confocal fluorescence microscopy images of CD31 staining. Scale bar: 100 μ m. (D), (E), and (F) are a quantitative comparison of fluorescence intensities in the slices of HIF-1 α staining from plot A, VEGF staining from plot B, and CD31 staining from plot C, respectively. * $p < 0.05$, ** $p < 0.01$, and *** $p < 0.001$.

Biocompatibility

The biocompatibility of PIBI-2240 was investigated using the RBW%, hepato-renal function, cytotoxicity, and hemolysis. As shown in Figure 7A, the RBW% of VX2 tumor-bearing rabbits exhibited slight changes 14 days after TAE treatment with PIBI-2240, Ivalon, and Lipiodol. The hepato-renal function indices, including ALT, AST, BUN, and CRE, were investigated in VX2 tumor-bearing rabbits on 0, 3, 6, and 14 days after hepatic arterial embolization (Figure 7B). The ALT and AST levels reached maximum values 3 days after treatment with Ivalon, Lipiodol, and PIBI-2240, signifying an acute hepatic injury. However, these values returned to normal levels 14 days after hepatic arterial embolization, but the renal function indices (BUN and CRE) remained almost unchanged 14 days after hepatic arterial as well as renal arterial embolization in normal rabbits (Figure S10). The cytotoxicity of PIBI-2240 was further compared with iohexol, Lipiodol, and PIBI-6150. The CV of PIBI-2240 was about 100% at an iodine concentration of 0.5–1,000 ng/mL, indicating that PIBI-2240 had the same cytotoxicity as that of iohexol and Lipiodol (Figure 7C). As shown in Figure 7D, the HRs of PIBI-2240, PIBI-6150, Lipiodol, and iohexol

were smaller than 5%, which indicated excellent blood compatibilities of $2.2 \pm 0.3\%$, $3.2 \pm 0.9\%$, $3.2 \pm 0.3\%$, and $1.8 \pm 0.5\%$, respectively.

Conclusions

In this study, we developed complex PIBI dispersions to address the issues of tumor collateral circulation and vascular re-canalization after TAE therapy. Using an IVIS Lumina XR system in X-ray mode, PIBI-2240 demonstrated a satisfactory X-ray attenuation ability. Furthermore, PIBI dispersions exhibited a temperature-sensitive transition between flowable sol phase and shrunken gel phase, of which CGC and CGT were affected by the mixing of iohexol. Compared to PIBI-6150 and Lipiodol, PIBI-2240 had a much higher temperature sensitivity and thus showed the best properties of flowability and embolization. A biomimetic model of tumor vasculature with two micro-fluidic chips was designed to investigate the *in vitro* artery-embolization properties. Complete embolization of all eight levels of micro-channels with sizes varying from 20 μ m to 800 μ m was achieved using PIBI-2240 compared to PIBI-6150 that has a higher viscosity making it difficult to diffuse into tiny capillaries (<200 μ m) and Lipiodol which has the eluting effect of PBS. Compared to Lipiodol and

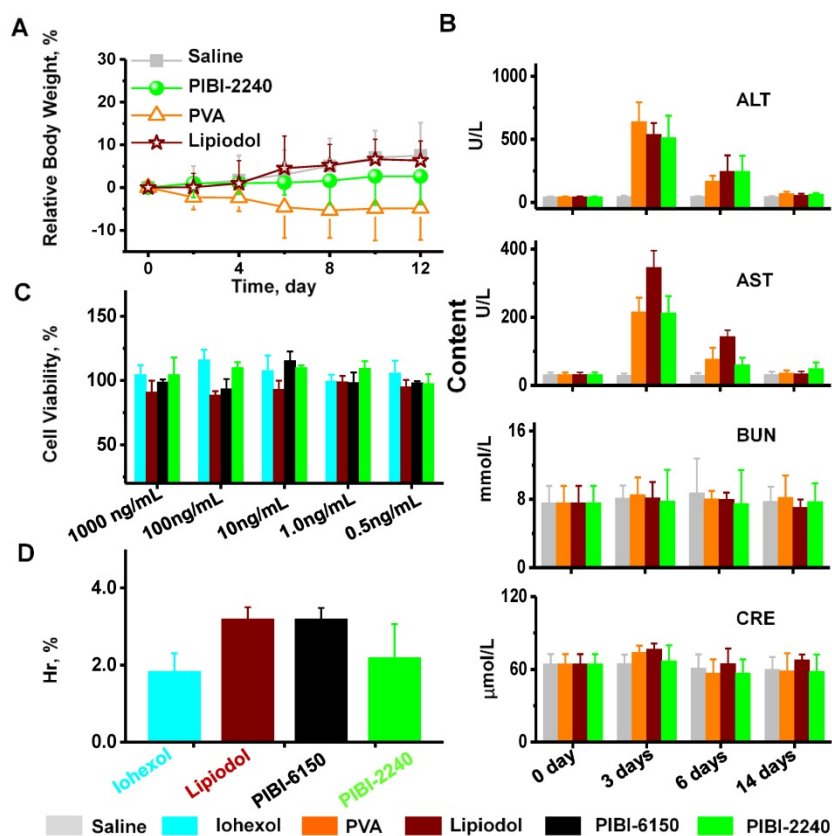


Figure 7. Biocompatibility evaluations of PIBI-2240. (A) The relative body weight changes of VX2 tumor-bearing rabbits during 14 days after various treatments. (B) Hepatorenal function of VX2 tumor-bearing rabbits at various time points after treatments. (C) Cytotoxicity comparison using the MTT assay on HepG2 cells ($n = 6$). (D) Hemolysis comparison ($n = 10$) of PIBI dispersions with Iohexol and Lipiodol. Saline (gray), PVA (orange), Lipiodol (burgundy), PIBI-6150 (black), PIBI-2240 (green).

Ivalon, PIBI-2240 achieved vessel-casting embolization of all levels of arteries in renal artery embolization in normal rabbits. The vessel-casting embolization effect significantly reduced the expression levels of HIF-1 α , VEGF, and CD31, which were often elevated because of the local hypoxia induced by Ivalon and Lipiodol in the TAE therapy. PIBI-2240 also achieved effective inhibition of tumor collateral circulation and vascular re-canalization and thus had the best anti-tumor effect of TAE therapy. With its excellent biocompatibility, PIBI-2240 shows promise as a novel blood-vessel-embolic material for tumor TAE therapy.

Abbreviations

TAE: transcatheter arterial embolization; TACE: transcatheter arterial chemo-embolization; HCC: hepatocellular carcinoma; HIF-1 α : hypoxia-inducible factor-1 α ; VEGF: vascular endothelial growth factor; PIB: poly(N-isopropylacrylamide-co-butyl methylacrylate); DLS: dynamic light scattering; TEM: transmission electron microscope; CGC: critical gelation concentration; CGT: critical gelation temperature; MRAs: main renal arteries; IRAs: intrarenal arteries; ARAs: afferent renal arteries; ALT:

alanine aminotransferase; AST: aspartate aminotransferase; BUN: blood urea nitrogen; CRE: serum creatinine; DSA: digital subtraction angiography; H&E: hematoxylin & eosin; TUNEL: terminal deoxynucleotidyl transferase (TdT)-mediated dUTP nick end labeling; DAPI: 4',6-diamidino-2-phenylindole dihydrochloride; MRI: magnetic resonance imaging.

Supplementary Material

Supplementary figures and tables.

<http://www.thno.org/v08p6291s1.pdf>

Supplementary movie 1.

<http://www.thno.org/v08p6291s2.mp4>

Supplementary movie 2.

<http://www.thno.org/v08p6291s3.mp4>

Supplementary movie 3.

<http://www.thno.org/v08p6291s4.mp4>

Supplementary movie 4.

<http://www.thno.org/v08p6291s5.mp4>

Acknowledgements

This work was supported by National Natural Science Foundation of China (grant No. 81673016, 81473171, 81471766 and 81571782), Shenzhen Science

and Technology Innovation Foundation (grant No. (2017)132), National Basic Research Program of China (973 Program, grant No. 2018YFA0208900, 2015CB931802) and PCSIRT (No. IRT13016). We also thank the Analysis and Test Center of HUST and School of Maters Engineering of HUST for related analysis.

Authors' contributions

YBZ, XLY and CSZ conceived the study. LL, YML and HL performed the experiments and carried out the analysis. LL, YML and HL designed the experiments and wrote the manuscript. All authors read and approved this submitted manuscript.

Competing Interests

The authors have declared that no competing interest exists.

References

- Wang S, Yang C, Zhang J, Kong XR, Zhu H, Wu F, et al. First experience of high-intensity focused ultrasound combined with transcatheter arterial embolization as local control for hepatoblastoma. *Hepatology*. 2014; 59: 170-7.
- Van der Sluis FJF, Bosch JL, Terkivatan T, Man R, Ijzermans JNM, Hunink MGM. Hepatocellular adenoma: cost-effectiveness of different treatment strategies. *Radiology*. 2009; 252: 737-46.
- Aqil A, Vasseur S, Duguet E, Passirani C, Benoit JP, Jerome R, et al. Magnetic nanoparticles coated by temperature responsive copolymers for hyperthermia. *J Mater Chem*. 2008; 18: 3352-60.
- Llovet JM, Real MI, Montana X, Planas R, Coll S, Aponte J, et al. Arterial embolization or chemoembolization versus symptomatic treatment in patients with unresectable hepatocellular carcinoma: a randomised controlled trial. *Lancet*. 2002; 359: 1734-9.
- Lo CM, Ngan H, Tso WK, Liu CL, Lam CM, Poon RT, et al. Randomized controlled trial of transarterial lipiodol chemoembolization for unresectable hepatocellular carcinoma. *Hepatology*. 2002; 35: 1164-71.
- Llovet JM, Di Bisceglie AM, Bruix J, Kramer BS, Lencioni R, Zhu AX, et al. Design and endpoints of clinical trials in hepatocellular carcinoma. *J Natl Cancer Inst*. 2008; 100: 698-711.
- Bruix J, Sherman M. Management of hepatocellular carcinoma: an update. *Hepatology*. 2011; 53: 1020-2.
- Sergio A, Cristofori C, Cardin R, Pivetta G, Ragazzi R, Baldan A, et al. Transcatheter arterial chemoembolization (TACE) in hepatocellular carcinoma (HCC): the role of angiogenesis and invasiveness. *Am J Gastroenterol*. 2008; 103: 914-21.
- Harris AL. Hypoxia—a key regulatory factor in tumor growth. *Nat Rev Cancer*. 2002; 2: 38-47.
- Von Marschall Z, Cramer T, Hocker M, Finkenzeller G, Wiedenmann B, Rosewicz S. Dual mechanism of vascular endothelial growth factor upregulation by hypoxia in human hepatocellular carcinoma. *Gut*. 2001; 48: 87-96.
- Kim YB, Park YN, Park C. Increased proliferation activities of vascular endothelial cells and tumor cells in residual hepatocellular carcinoma following transcatheter arterial embolization. *Histopathology*. 2001; 38: 160-6.
- Kai AK, Chan LK, Lo RC, Lee JM, Wong CC, Wong JC, et al. Down-regulation of TIMP2 by HIF-1alpha/miR-210/HIF-3alpha regulatory feedback circuit enhances cancer metastasis in hepatocellular carcinoma. *Hepatology*. 2016; 64: 473-87.
- Liang B, Zheng CS, Feng GS, Wu HP, Wang Y, Zhao H, et al. Experimental evaluation of inhibitory effect of 10-hydroxycamptothecin on hypoxia-inducible factor-1alpha expression and angiogenesis in liver tumors after transcatheter arterial embolization. *J Vasc Interv Radiol*. 2010; 21: 1565-72.
- Longchamp A, Mirabella T, Arduini A, MacArthur MR, Das A, Trevino-Villarreal JH, et al. Amino acid restriction triggers angiogenesis via GCN2/ATF4 regulation of VEGF and H2S production. *Cell*. 2018; 173: 117-29.
- Guan YS, He Q, Wang MQ. Transcatheter arterial chemoembolization: history for more than 30 years. *ISRN Gastroenterol*. 2012; 2012: 480650.
- Wang DX, Gaba RC, Jin B, Lewandowski RJ, Riaz A, Memon K, et al. Perfusion reduction at transcatheter intraarterial perfusion MR imaging: a promising intraprocedural biomarker to predict transplant-free survival during chemoembolization of hepatocellular carcinoma. *Radiology*. 2014; 272: 587-97.
- Fornier A, Llovet JM, Bruix J. Hepatocellular carcinoma. *Lancet*. 2012; 379: 1245-55.
- Lencioni R, de Baere T, Soulen MC, Rilling WS, Geschwind JF. Lipiodol transarterial chemoembolization for hepatocellular carcinoma: A systematic review of efficacy and safety data. *Hepatology*. 2016; 64: 106-16.
- Ronald J, Nixon AB, Marin D, Gupta RT, Janas G, Chen W, et al. Pilot evaluation of angiogenesis signaling factor response after transcatheter arterial embolization for hepatocellular carcinoma. *Radiology*. 2017; 285: 311-8.
- De Baere T, Arai Y, Lencioni R, Geschwind JF, Rilling W, Salem R, et al. Treatment of liver tumors with lipiodol TACE: technical recommendations from experts opinion. *Cardiovasc Intervent Radiol*. 2016; 39: 334-43.
- Louail B, Sapoval M, Bonneau M, Wasseff M, Senechal Q, Gaux JC. A new porcine sponge material for temporary embolization: an experimental short-term pilot study in swine. *Cardiovasc Intervent Radiol*. 2006; 29: 826-31.
- Cabrera R, Dhanasekaran R, Caridi J, Clark V, Morelli G, Soldevila-Pico C, et al. Impact of transarterial therapy in hepatitis C-related hepatocellular carcinoma on long-term outcomes after liver transplantation. *Am J Clin Oncol*. 2012; 35: 345-50.
- Lencioni R, Crocetti L. Local-Regional treatment of hepatocellular carcinoma. *Radiology*. 2012; 262: 43-58.
- Lee MY, Chuang VP, Wei CJ, Cheng TY, Cherng MT. Histopathologic correlation of hepatocellular carcinoma after transcatheter arterial chemoembolization with polyvinyl alcohol particle of various sizes. *Eur J Radiol*. 2012; 81: 1976-9.
- Li Q, Ao GK, Duan F, Wang ZJ, Yan JY, Wang MQ. Incidence and therapeutic frequency of extrahepatic collateral arteries in transcatheter arterial chemoembolization of hepatocellular carcinoma: Experience from 182 patients with survival time more than 3 years. *Eur J Radiol*. 2015; 84: 2555-63.
- Raymond J, Metcalfe A, Leblanc P, Salazkin I, Papineau K, Roy D, et al. Production of radioactive particles for endovascular therapeutic interventions. *Biomaterials*. 2006; 27: 1566-72.
- Marelli L, Stigliano R, Triantos C, Senzolo M, Cholongitas E, Davies N, et al. Transarterial therapy for hepatocellular carcinoma: which technique is more effective? A systematic review of cohort and randomized studies. *Cardiovasc Intervent Radiol*. 2007; 30: 6-25.
- Zhao YB, Zheng CS, Wang Q, Fang JL, Zhou GF, Zhao H, et al. Permanent and peripheral embolization: temperature-sensitive p(N-Isopropylacrylamide-co-butyl methylacrylate) nanogel as a novel blood-vessel-embolic material in the interventional therapy of liver tumors. *Adv Funct Mater*. 2011; 21: 2035-42.
- Qian K, Ma YY, Wan JS, Geng SN, Li H, Fu QW, et al. The studies about doxorubicin-loaded p(N-isopropyl-acrylamide-co-butyl methylacrylate) temperature-sensitive nanogel dispersions on the application in TACE therapies for rabbit VX2 liver tumor. *J Control Release*. 2015; 212: 41-9.
- Xiong W, Wang W, Wang Y, Zhao YB, Chen HB, Xu HB, et al. Dual temperature/pH-sensitive drug delivery of poly(N-isopropylacrylamide-co-acrylic acid) nanogels conjugated with doxorubicin for potential application in tumor hyperthermia therapy. *Colloids Surf B Biointerfaces*. 2011; 84: 447-53.
- Ma YY, Wan JS, Qian K, Geng SN, He NJ, Zhou GF, et al. The studies on highly concentrated complex dispersions of gold nanoparticles and temperature-sensitive nanogels and their application as new blood-vessel-embolic materials with high-resolution angiography. *J Mater Chem B*. 2014; 2: 6044-53.
- Chen XH, Zhao YB, Geng SN, Miron RJ, Zhang Q, Wu CT, et al. In vivo experimental study on bone regeneration in critical bone defects using PIB nanogels/boron-containing mesoporous bioactive glass composite scaffold. *Int J Nanomedicine*. 2015; 10: 839-46.
- Wan JS, Geng SN, Zhao H, Peng XL, Zhou Q, Li H, et al. Doxorubicin-induced co-assembling nanomedicines with temperature-sensitive acidic polymer and their in-situ-forming hydrogels for intratumoral administration. *J Control Release*. 2016; 235: 328-36.
- Zhao H, Xu JB, Wan JS, Geng SN, Li H, Peng XL, et al. Cisplatin-directed coordination-crosslinking nanogels with thermo/pH-sensitive triblock polymers: improvement on chemotherapeutic efficacy via sustained release and drug retention. *Nanoscale*. 2017; 9: 5859-71.
- Tak E, Lee S, Lee J, Rashid MA, Kim YW, Park JH, et al. Human carbonyl reductase 1 upregulated by hypoxia renders resistance to apoptosis in hepatocellular carcinoma cells. *J Hepatol*. 2011; 54: 328-39.
- Fan Y, Potdar AA, Gong Y, Eswarappa SM, Donnola S, Lathia JD, et al. Profilin-1 phosphorylation directs angiocrine expression and glioblastoma progression through HIF-1alpha accumulation. *Nat Cell Biol*. 2014; 16: 445-56.
- Spencer JA, Ferraro F, Roussakis E, Klein A, Wu J, Runnels JM, et al. Direct measurement of local oxygen concentration in the bone marrow of live animals. *Nature*. 2014; 508: 269.
- Qian Y, Song JL, Zhao XT, Chen W, Ouyang YM, Yuan WE, et al. 3D fabrication with integration molding of a graphene oxide/polycaprolactone nanoscaffold for neurite regeneration and angiogenesis. *Adv Sci*. 2018; 5: 1-18.
- Biswas S, Charlesworth PJ, Turner GD, Leek R, Thamboo PT, Campo L, et al. CD31 angiogenesis and combined expression of HIF-1alpha and HIF-2alpha are prognostic in primary clear-cell renal cell carcinoma (CC-RCC), but HIF1alpha transcriptional products are not: implications for antiangiogenic trials and HIF1alpha biomarker studies in primary CC-RCC. *Carcinogenesis*. 2012; 33: 1717-25.

40. Gupta B, Chiang L, Chae K, Lee DH. Phenethyl isothiocyanate inhibits hypoxia-induced accumulation of HIF-1 α and VEGF expression in human glioma cells. *Food Chem.* 2013; 141: 1841-6.
41. Xu HQ, Li B, Yu WJ, Wang H, Zhao XF, Yao YC, et al. Correlation between F-18-FDG uptake and the expression of glucose transporter-1 and hypoxia-inducible factor-1 α in transplanted VX2 tumors. *Nucl Med Commun.* 2013; 34: 953-8.
42. Dai F, Zhang XM, Shen WR, Chen J, Liu LC, Gao GJ. Liposomal curcumin inhibits hypoxia-induced angiogenesis after transcatheter arterial embolization in VX2 rabbit liver tumors. *Oncol Targets Ther.* 2015; 8: 2601-11.
43. Sharma KV, Bascal Z, Kilpatrick H, Ashrafi K, Willis SL, Dreher MR, et al. Long-term biocompatibility, imaging appearance and tissue effects associated with delivery of a novel radiopaque embolization bead for image-guided therapy. *Biomaterials.* 2016; 103: 293-304.
44. Poursaid A, Price R, Tiede A, Olson E, Huo E, McGill L, et al. In situ gelling silk-elastinlike protein polymer for transarterial chemoembolization. *Biomaterials.* 2015; 57: 142-52.
45. Zheng Y, Chen JM, Craven M, Choi NW, Totorica S, Diaz-Santana A, et al. In vitro microvessels for the study of angiogenesis and thrombosis. *Proc Natl Acad Sci U S A.* 2012; 109: 9342-7.
46. Rong JJ, Liang M, Xuan FQ, Sun JY, Zhao LJ, Zhen HZ, et al. Alginate-calcium microsphere loaded with thrombin: a new composite biomaterial for hemostatic embolization. *Int J Biol Macromol.* 2015; 75: 479-88.
47. Wang Q, Qian K, Liu SS, Yang YJ, Liang B, Zheng CS, et al. X-ray visible and uniform alginate microspheres loaded with in situ synthesized BaSO₄ nanoparticles for in vivo transcatheter arterial embolization. *Biomacromolecules.* 2015; 16: 1240-6.
48. Murray CD. The physiological principle of minimum work II Oxygen exchange in capillaries. *Proc Natl Acad Sci U S A.* 1926; 12: 299-304.
49. Golfieri R, Cappelli A, Cucchetti A, Piscaglia F, Carpenzano M, Peri E, et al. Efficacy of selective transarterial chemoembolization in inducing tumor necrosis in small (<5 cm) hepatocellular carcinomas. *Hepatology.* 2011; 53: 1580-9.
50. Li GP, Ye L, Pan JS, Long MY, Zhao ZZ, Yang HY, et al. Antitumoral hydroxyapatite nanoparticles-mediated hepatoma-targeted trans-arterial embolization gene therapy: in vitro and in vivo studies. *Liver Int.* 2012; 32: 998-1007.
51. Yan X, Wu C, Chen T, Santos MM, Liu CL, Yang C, et al. Cathepsin S inhibition changes regulatory T-cell activity in regulating bladder cancer and immune cell proliferation and apoptosis. *Mol Immunol.* 2017; 82: 66-74.
52. Liu YM, Peng XL, Qian K, Ma YY, Wan JS, Li H, et al. Temperature sensitive p(N-isopropylacrylamide-co-acrylic acid) modified gold nanoparticles for trans-arterial embolization and angiography. *J Mater Chem B.* 2017; 5: 907-16.
53. Hoogenboom R. Poly(2-oxazoline)s: a polymer class with numerous potential applications. *Angew Chem Int Ed Engl.* 2009; 48: 7978-94.
54. Zhao H, Zheng CS, Feng GS, Zhao YB, Liang HM, Wu H, et al. Temperature-sensitive poly(N-isopropylacrylamide-co-butyl methylacrylate) nanogel as an embolic agent: distribution, durability of vascular occlusion, and inflammatory reactions in the renal artery of rabbits. *AJNR Am J Neuroradiol.* 2013; 34: 169-76.